

# A statistical study of spots in torsional Couette flow

Le Gal Patrice<sup>†</sup>, Tasaka Yuji<sup>††</sup>, Nagao Jotaro<sup>††</sup>, Cros Anne<sup>†</sup> and Yamaguchi Kohei<sup>††</sup>

<sup>†</sup>*Institut de Recherche sur les Phénomènes Hors Equilibre, UMR 6594, CNRS & Universités d'Aix-Marseille I et II, 49 rue F. Joliot-Curie, BP146, 13384 Marseille, France.*

<sup>††</sup>*Laboratory for Flow Control, Graduate School of Engineering, Hokkaido University, N-13 W-8, 060-8628 Sapporo, Japan.*

July 19, 2006

**Abstract.** This article presents some results on the statistical behavior of localized structures - called "spots" - that propagate in the flow between a rotating and a stationary disc when those are very close one to the other. Under these conditions the rotating disc flow belongs to the Couette flow family and is called the torsional Couette flow. Some visualizations of its transition to turbulence have already revealed the propagation of these spots [Schouveiler et al., J. Fluid Mech. 443, pp. 329-350, 2001] from the rim of the disc towards its center. Using flow visualizations and an original image analysis, the present study aims to better describe the characteristics of the spots whose number continuously increases with the Reynolds number until they invade the whole flow. Moreover, we propose a statistical model that predicts an error function shape for the probability to observe a spot at a given radial position. This prediction is confirmed by an image analysis of the flow and the stability curve of torsional Couette flow is deduced from these observations.

**Keywords:** transition to turbulence, rotating flows

## 1. Subcritical transition of the Couette flow family

One of the most amazing features of fluid mechanics is certainly the transition to turbulence of plane Couette flow (PCF). This two-dimensional laminar shear flow is created in the gap between two parallel plates when one of the plates is translated at a constant velocity. The velocity profile in the direction perpendicular to the plates is a linear function of the distance to the fixed plate as shown in figure 1-a). Despite the extreme simplicity of this flow, its transition to turbulence is still an open question of fluid mechanics although recent important progresses have been realized. In particular Prigent *et al.* (1) have shown that turbulence appears as periodic inclined bands in the laminar flow before it invades the whole flow. These bands whose origins and characteristics are not yet understood, have however been reproduced in numerical simulations by Barkley and Tuckerman (2). In fact, it was shown by Prigent *al.* that this banded turbulence has the same threshold, wavenumber and inclination angle with respect to

*Figure 1.* The three members of the Couette flow family. a) the plane Couette flow between two planes, b) the Taylor-Couette flow between two cylinders, c) the torsional Couette flow between two discs.

the streamwise direction, as the spiral turbulence discovered forty years ago by Coles (3) and van-Atta (4) in the Taylor-Couette flow (TCF). Indeed, the Taylor-Couette flow between two rotating co-axial cylinders is, in the small gap approximation, similar to the plane Couette flow as can be seen in figure 1-b). Consequently, the turbulent bands of the PCF are the exact equivalents of the turbulent spirals of the TCF. More recently, a third type of flow was added to this Couette family and its banded turbulence: it was shown (5) that the gap flow between a rotating and a stationary disc is subject to spatio-temporal intermittency that is created by the presence of turbulent spirals (true spirals this time and not helices as it is often said for the TCF). As for the TCF flow inside coaxial cylinders, the small gap approximation for this flow is again the Couette flow (see figure 1-c). The main ingredient to get this original transition to turbulence comes from the property of the three flows to be bistable: the laminar flows are linearly stable (at least in a certain range of Reynolds numbers) but they are unstable against finite size perturbations at relatively small Reynolds numbers. The flows can then bifurcate towards states characterized by strongly non linear localized turbulent patches inside laminar domains. At higher Reynolds numbers, these patches develop into the turbulent bands. Moreover, it was shown by Dauchot and Daviaud (6) that there is a minimum critical amplitude for perturbations to be sustained in the plane Couette flow. This minimum amplitude  $A_c$  is a function of the Reynolds number  $Re$ : at high Reynolds numbers, the laminar flow is more susceptible to be destabilized than at small Reynolds numbers. Therefore,  $A_c = f(Re)$  is a monotonically decreasing curve as drawn in figure 2. This curve is called the stability curve and Dauchot and Daviaud (6) have also shown that there is a maximum Reynolds number under which perturbations (that we suppose to be generic) cannot grow. Therefore, they confirm the general power law behavior of the stability curve:  $A_c = (Re - Re_c)^\alpha$ . In particular, this defines a global stability critical Reynolds number  $Re_c$  which is equal to  $1300 \pm 20$  in PCF (with our definition of the Reynolds number, see later). The determination of the exponent  $\alpha$  was the subject of several studies and it seems that there is today a general agreement for a value of  $\alpha$  between  $-1$  and  $-7/4$  as predicted by different studies (7; 8). A semi-realistic model of PCF shows also that this exponent is equal to  $-1$  (9). Note that an exponent of  $-1$  was obtained by Waleffe from a simple balance between non linear advection terms and viscous terms (10). More recently, it was

shown that this exponent  $\alpha$  is between  $-1$  (11) and  $-1.4$  (12) in a pipe flow transition to turbulence which is also known to be subcritical .

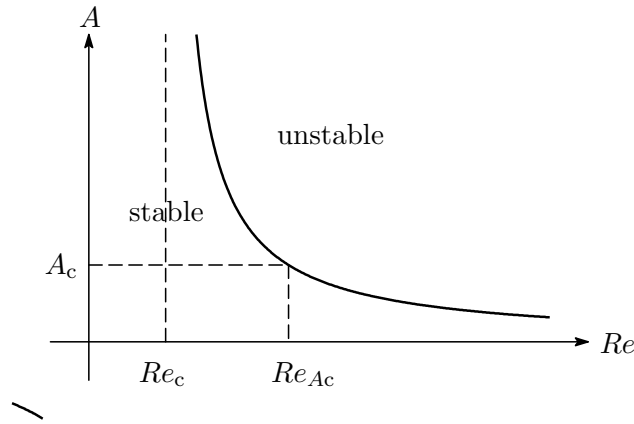


*Figure 2.* The stability curve for finite amplitude perturbations to be sustained in the flows of the Couette family. Perturbations are damped if their amplitudes are lower than the critical amplitude  $A_c$  that corresponds to a critical Reynolds number  $Re_{Ac}$ . A generic shape for this curve is given by a power law  $A_c = (Re - Re_c)^\alpha$ .

As regards the torsional Couette flow, Cros and Le Gal (5) showed that the transition to turbulence via the turbulent spirals was in fact blocked to a maximum turbulent fraction equal to  $1/2$ . A relaminarization of the flow was even observed at higher rotation speeds. The final transition process occurs by the nucleation of a growing number of tiny localized structures which were referred to "spots" by Schouveiler et al. (13). Their appearance threshold is a function of the distance  $h$  between the discs and of the rotation rate  $\Omega$  of the rotating disc. Figure 3-a) represents a snap-shot of this flow where spots can be observed as small black areas. They have a "V" shape with the legs turned towards the disc rotation direction and thus look like the horse-shoe vortices classically observed in boundary layers (see figure 3-c). In our case, the legs would be pinned to the rotating disc and the head of the structure would be transported by the mean flow at proximity of the fixed disc. We suspect that they are generated on natural fluctuations of random amplitude close to the rim of the disc at a radius  $R$ . Then, they propagate through the laminar flow along a spiral towards the center of the flow (see figure 3-b). The spiral rolls up towards the center of the flow in the same direction as the disc rotation. Their size is approximately given by  $h$  and we have observed that they never propagate farther than a critical radius for a given Reynolds number. The determination of this critical radius will be the subject of section 4. The total number of spots

increases and they propagate further towards the center as the rotation speed  $\Omega$  is increased. The ultimate turbulent state is then formed when a large number of spots amalgamate. As already described, the torsional

*Figure 3.* a) Visualization of spots in the torsional Couette flow. b) Schematic representation of the spot spiraling path from the disc rim to the disappearance radius  $r_A$ . c) close-up of the spots where the "v" shape with the two legs reminiscent of a horse shoe vortical structure is visible; two different regions of the flow are presented.

Couette flow is formed when the rotating boundary layer (the Kármán layer) and the stationary disc layer (the Bödewadt layer) merge. Note that this is only possible (at the considered Reynolds numbers) when the stationary and the rotating disc are sufficiently close to one another, otherwise another transition that involves circular and spiral waves takes place (14). Because of rotation, the velocity field is three-dimensional and a centrifugal flow takes place in the Karman layer. Due to mass conservation, a centripetal flow is then also present in the Bödewadt layer and creates what is often referred as Ekman pumping. Therefore, we suspect that the spots which are generated at the disc periphery, on natural uncontrolled fluctuations of amplitude  $A$ , are transported towards the center by this re-circulating flow. Then, as the local Reynolds number is directly proportional to the radial position on the disc ( $Re = 2\pi\Omega rh/\nu$ ,  $\nu$  being the fluid viscosity), the spots experience a decreasing Reynolds number until they meet a threshold  $R_{Ac}$  and die at radius  $r_{Ac}$ .

The aim of this study is to provide a statistical description of this transition to turbulence and to obtain the stability curve  $A_c = f(Re)$  for torsional Couette flow. To this end, recordings of flow visualization experiments will be analyzed by means of image processing techniques.

## 2. The apparatus and the visualization technique

Figure 4 is a schematic representation of the main part of the device used in this study. The enclosure, which contains the fluid used in this experiment (water at room temperature around 20°C) is cylindrical, with a radius of 152 mm and a depth of 60 mm. The stainless steel rotating disc is immersed in this container and possesses a radius  $R = 150$  mm and a thickness of 13 mm. This disc is set into rotation by a D.C. electric motor. The rotational speed  $\Omega$  is controlled and regulated within 0.2% via a feedback control loop.  $\Omega$  can vary between 0 and 200 rpm. The second adjustable control parameter is the distance  $h$  between the two discs that can be continuously adjusted between 0

and 21 mm with an accuracy of 0.02 mm. The stationary disc is the removable lid of the tank. It is made in a transparent 20 mm thick plexiglass plate that permits to visualize the flow. There is a radial gap  $dr$  between the cylindrical wall of the container and the disc.  $dr$  is adjustable between 0.1 mm and 2 mm by means of plastic thin rings which are adjusted around the rotating disc in order to change its diameter and consequently the radial gap. This enables modifying the lateral boundary conditions of the rotating flow. The tank is completely filled with water and a hole in the center of the lid facilitates removing air bubbles trapped underneath the lid. After all air is removed from water, the hole is sealed before the experiment begins. Water temperature is measured during the experiment and viscosity corrections are taken into account to calculate the Reynolds numbers, but only weak temperature deviations, less than 2 degrees, have been observed.

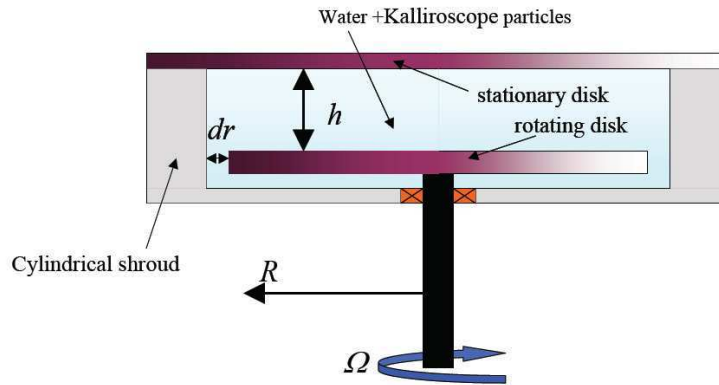
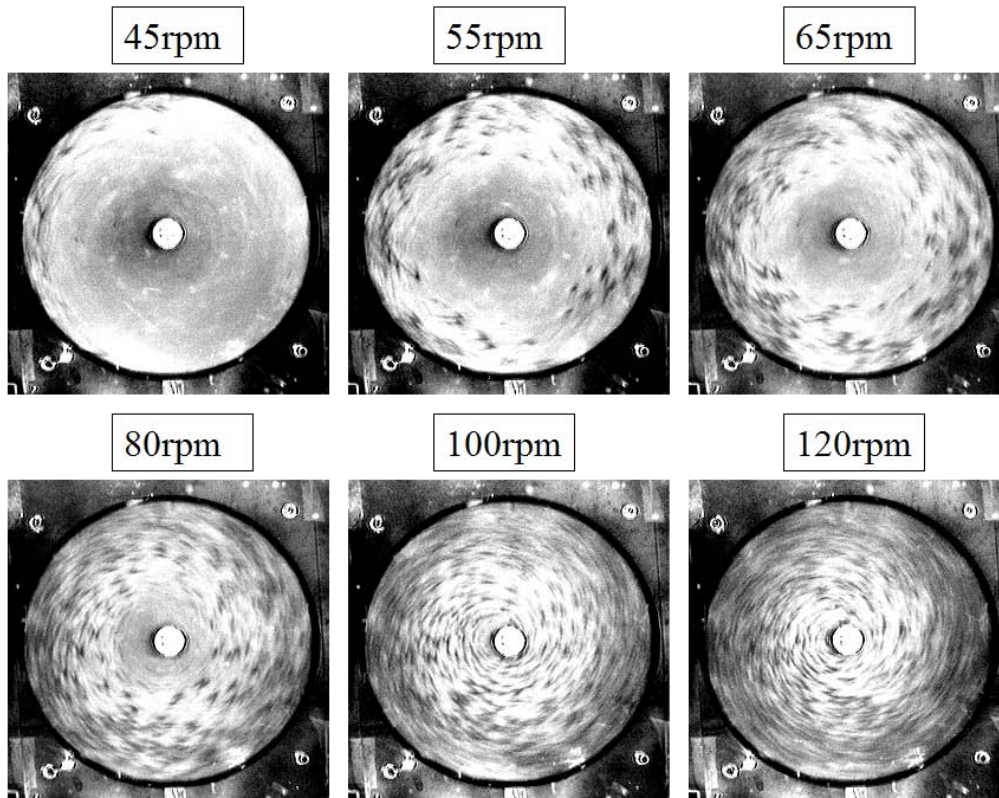


Figure 4. The rotating disc device. The disc has a radius  $R$  of 150mm, the gap distance  $h$  between the disc and the stationary lid can vary between 1 and several mm. The radial gap  $dr$  between the disc and the stationary cylindrical shroud can be varied between 0.1 and 2mm by means of thin additional rings.

In order to visualize the flow, water is seeded by anisotropic and reflective Kalliroscope particles<sup>1</sup>. Those constitute a poly-dispersive solution of flat flakes having a typical size of  $30 \times 6 \times 0.07 \mu\text{m}$ . Kalliroscope fluid is added to water in a proportion of 1% to 3% in weight. The orientation of the particles depends on the local shear (15; 16) and this characteristic facilitates this well-known visualization technique. As the disc is painted in black, the orientation fluctuations of the particles inside spots result in the visualization of these as dark areas. The flow is illuminated by the means of ten bulbs positioned on a 50 cm diameter circle, equally spaced and located approximately 1 m above the disc.

<sup>1</sup> [www.kalliroscope.com](http://www.kalliroscope.com)



*Figure 5.* Visualization of the transition to turbulence of the torsional Couette flow ( $h = 2.8$  mm). When the rotating frequency is increased, the number of spots increases and their observation minimum radius decreases. Disc rotation is clockwise.

The flow is filmed by a video camera placed 1 m above the discs and aligned with the axis of rotation. This camera is connected to a PC and a frame grabber permits to record video movies and images of the flow. These movies are analyzed by means of an image-analysis software developed in our research group.

### 3. Visualization and analysis of spots nucleation

Figure 5 presents a typical series of images illustrating the transition to turbulence of the torsional Couette flow. As previously observed, the spots appear on images as black V shaped areas. Depending on the illumination, or of the quantity of Kalliroscope particles or the dark shadow of the central cap, a grey central zone may be visible in

some of the runs. This grey central zone (where the flow is strictly laminar and free of spots) will be removed from the image in order to perform the statistical study of section 3. As can be observed, the number of spots increases as  $\Omega$  is increased and they propagate further towards the center of the flow. For each  $h$ , the first spot appears at a critical  $\Omega$ . Therefore the flow parameters where spots are observed can be determined by visual inspection analogous to the procedures in ref. (5). As the spots are created in the region of the flow next to the radial gap, we performed an exhaustive study of the influence of the radial gap size on the spot creation. As expected,  $dr$  affects the appearance of spots and figure 6-a) shows the influence of this gap width on the critical Reynolds number ( $2\pi\Omega R h/\nu$ , where  $R$  is the radius of the rotating disc) where the spots appear. These measurements have been performed for each gap distance  $h$ . We performed four experiments ( $dr = 0.65, 1.25, 1.5$  and  $2$  mm) and the results obtained by Schouveiler *et al* (13) for  $dr = 0.1$  mm are also included in the figure. Figure 6 clearly shows that the gap size is a key parameter in the formation of spots and that the threshold is pushed to higher Reynolds numbers as the gap decreases as can be seen on figure 6-b). This result shows that the flow in the proximity of the radial gap, generates fluctuations that are susceptible to growth if the Reynolds number is large enough. Then, these perturbations rapidly evolve towards the horse-shoe structure of spots and they are transported with the centripetal flow. Figure 6-a) also confirms that the spots thresholds do not vary with  $h$  (at least in the explored range) proving that finite size effects do not interfere significantly in the transition process, except of course for generating the initial perturbations in the radial gap.

*Figure 6.* a) Critical Reynolds number threshold for spot appearance as a function of the distance  $h$  between the discs and parameterized by the radial gap  $dr$  between the disc and the cylindrical shroud.  $\star$   $dr = 2$  mm;  $\times$   $dr = 1.5$ mm;  $+$   $dr = 1.25$ mm;  $\circ$   $dr = 0.65$ mm;  $\triangle$   $dr = 0.1$  mm from (13); b) Variation of the critical Reynolds number (averaged on  $h$ ) with the radial gap size  $dr$ .

Together with this threshold determination, we have also counted the number of spots as a function of the Reynolds number based on the disc radius. The spots were counted by visual inspection of series of successive images. Strong fluctuations of the number of spots are apparent from the data of figure 7. These data represent a temporal series (for  $\Omega = 55$  rpm) where several bursts of a large number of spots appear from time to time. The histogram of this series is also presented in figure 7. As can be seen, it displays a long tail of rare events - a feature reminiscent of a Poisson distribution.

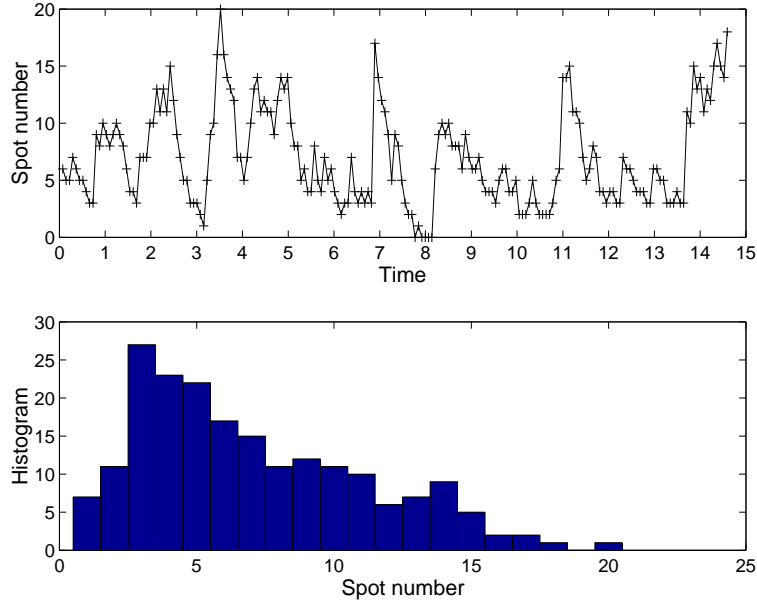


Figure 7. top: Temporal series (time unit is the disc rotation period) of spot number for  $\Omega = 55$  rpm and  $h = 3.1$  mm. Strong intermittency is observable with some burstings of groups of spots. bottom: Histogram of the temporal series that shows a Poisson like distribution of the spot occurrence.

The evolution of the time averaged number  $\langle n \rangle$  of spots versus  $\Omega$  is presented in figure 8 for  $h = 3$  mm and in the top figure and for  $h = 3.1$  mm for the middle plot. The global threshold for the first emergence of spots is easily determined although the number of spots fluctuates substantially. The error bars represent in fact the standard deviation  $\sqrt{\langle n^2 \rangle}$  of the temporal series. It is observed that the data displays two distinct regions in which  $\langle n \rangle$  increases approximately linearly but at different rates. This fact was systematically confirmed on every run. As a means to test the assumption that the histogram in figure 7 displays a Poisson distribution for the occurrence of spots, we have plotted the evolution of this variance  $\langle n^2 \rangle$  as a function of the mean number of spots  $\langle n \rangle$  in figure 8 (bottom). It can be seen that, except for a single run, the data align perfectly on a straight line as it is characteristic for a Poisson distribution. This corroborates the statistical independence of the spots which consist of, as expected, fast (the life time of a spot is about one tenth of a rotating period) isolated random events. Note that the run at  $\langle n \rangle = 11$  which lies quite substantially above the line extrapolating the other data points in figure 8 (bottom) is also the run where  $\langle n \rangle$  changes its evolution. We

have no explanation for this slope change which has been systematically observed in experimental runs for different values of  $h$ .

*Figure 8.* Evolution of the average number of spots as a function of the rotation speed  $\Omega$  for  $h = 3$  mm (top) and for  $h = 3.1$  mm (middle). Test of the Poisson law where the variance  $\langle n^2 \rangle$  is equal to the mean number of spots  $\langle n \rangle$  (except for  $\Omega = 58$  rpm) for  $h = 3.1$  mm (bottom).

#### 4. Statistical analysis by image processing

In order to perform a more accurate statistical description of the behavior of the spots, an image analysis has been performed to determine the distribution of spots as a function of  $r$ . Figure 9-a) shows an example of an image of the flow displaying a large number of spots. These spots are represented by a group of darker pixels. Such a light intensity variation can be quantified by the determination at each pixel of its brightness  $I$ . In the RGB system, a video image taken by a CCD camera can be expressed at each pixel by its three color components: Red  $R$ , Green  $G$  and Blue  $B$ . Using a classical definition of the intensity  $I$  of the brightness of a pixel, one can calculate  $I$  from these three components to be equal to  $I = 0.299R + 0.587G + 0.114B$  (this definition comes in fact from the best human color perception (17)). In order to extract individual spots, a binarization technique, which classifies pixels into two sets, darker or brighter pixels, was performed. Figure 9-b) is the binary image of Figure 9-a) using a threshold, which is determined by Otsu's method (17). This threshold value is chosen when the covariance between two separated sets of different brightness intensity probability distribution becomes a maximum. The covariance  $\sigma_B^2$  for a given threshold  $k$  between set 1 and set 2 is determined as

$$\begin{aligned}\sigma_B^2(k) &= (\mu_1 - \mu_T)^2\omega_1 + (\mu_2 - \mu_T)^2\omega_2 \\ &= \omega_1\omega_2(\mu_1 - \mu_2)^2,\end{aligned}\tag{1}$$

where  $\mu_1$  and  $\mu_2$  are the averaged brightness values of set 1 and set 2 respectively and where  $\mu_T$  is the average brightness value for the whole binary image. Similarly,  $\omega_1$  and  $\omega_2$  are the probability of each set defined as:

$$\omega_1 = \sum_{i=0}^k p_i, \quad \omega_2 = \sum_{i=k+1}^{255} p_i = 1 - \omega_1 \quad \text{with} \quad \sum_{i=0}^{255} p_i = 1.$$

where  $p_i$  is the probability distribution of the brightness intensity.

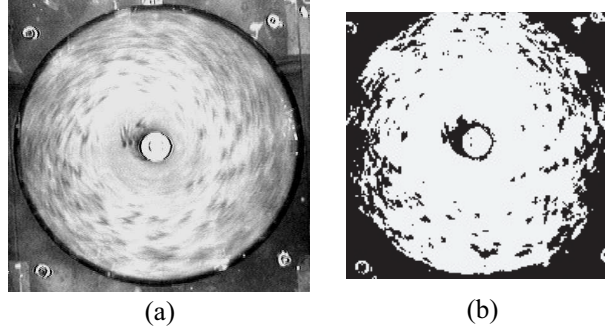


Figure 9. An example of a raw image (a) and its corresponding binary image (b) from Kalliroscope flow visualization.

The probability for a spot to exist at radial position  $r$  is determined by  $P(r) = N_b/N$  where  $N$  is the number of pixels calculated on a circle of radius  $r$  and  $N_b$  the total number of black pixels on the circle.  $P(r)$  also represents the product of the average size of a spot and the number of spots on a circle. Such an analysis has been performed by averaging  $P(r)$  on a large number of images (typically 50), for different speeds of rotation  $\Omega$  and different axial gap distances  $h$  and for a fixed radial gap  $dr = 2$  mm. Figure 10 shows these probability distributions as functions of the flow parameters. As expected,  $P(r)$  increases with respect to the radial position  $r$  and also with the rotation speed  $\Omega$ . Near the rim of the disk, we can observe that spots are in their formation process ( $P(r)$  increases or decreases sharply) before a plateau is formed around  $r/R = 0.9$ . Note that, as already mentioned, the central part of the flow can be polluted by the dark shadow of the cap in the middle of the lid. Consequently, only values of  $r/R$  larger than 0.4 will be considered in the following. Moreover, the two runs where high levels of grey are visible ( $h = 2.4$  mm,  $\Omega = 90$  rpm and  $\Omega = 100$  rpm) will not be used in the following statistical analysis.

Figure 10. Probability  $P(r)$  to get a black pixel for different value of  $\Omega$  and  $h$ . The radial gap  $dr$  is fixed to 2 mm ( top-left,  $h = 2.4$  mm; top-right,  $h = 2.6$  mm; bottom-left,  $h = 2.8$  mm; bottom-right,  $h = 3$  mm).

The main goal of the following analysis is to determine the stability curve of torsional Couette flow from these  $P(r)$  curves. These curves can be interpreted as the response of the flow against external random perturbations. We will develop a model for spot propagation in order to determine in particular if the spots disappear at a typical critical radius that depends on their amplitude. To this end, we first assume that the stability curve of torsional Couette flow is similar to that of

2-D Couette flow as shown in Figure 2, the local Reynolds number being directly converted into the radial position  $r$ . As we saw before, spots are generated by the growth of perturbations close to the radial gap between the rotating disc and the cylindrical wall. When created, a spot travels on a spiralling path towards the center of the flow. Its amplitude  $A$  is an unknown function of  $r$  as illustrated in figure 11. It is therefore probable that the distribution  $Prob(A)$  of the amplitudes of the perturbations or of the spots (when created) also varies with  $r$ .

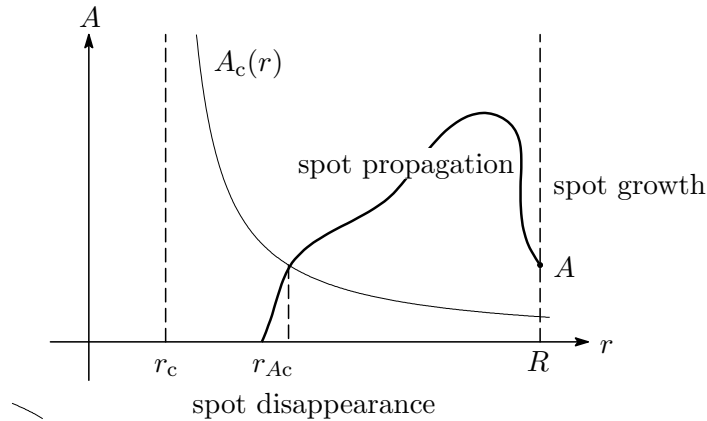


Figure 11. Schematic diagram of amplitude  $A$  variation with respect to  $r$ .

We define  $P_A(r, t)$  as the probability to observe a spot of a given amplitude  $A$ , at radius  $r$  and at time  $t$ . If one averages this quantity over time, the probability for observing spots of amplitude  $A$  on a circle of radius  $r$  is  $P_A(r) = \langle P_A(r, t) \rangle_t$ . If the spots had a unique amplitude  $A$ , because of the determinism of the Navier-Stokes equations, it is straightforward to deduce that  $P_A(r)$  would be a step function located in  $r = r_{Ac}$ . As illustrated in figure 12, the totality of identical spots created on identical fluctuations would disappear at the same critical radius  $r_{Ac}$ . We assume here that the relaxation time of damped spots for  $r < r_{Ac}$ , is shorter than their lifetime so that we neglect the duration the spots will take to completely disappear after they cross the stability radius. In fact, the estimation of the damping rate of a spot after it has crossed the critical radius is not obvious. However, this assumption is supported by the visual study of spots that shows that they keep a constant V shape (and apparently constant amplitude) all along their trajectory until they abruptly disappear.

In fact, each spot is associated with a particular value  $A$  for the amplitude of the perturbations. Thus there is a probability distribution  $Prob(A)$  for the statistic variable  $A$ . Figure 13 illustrates furthermore

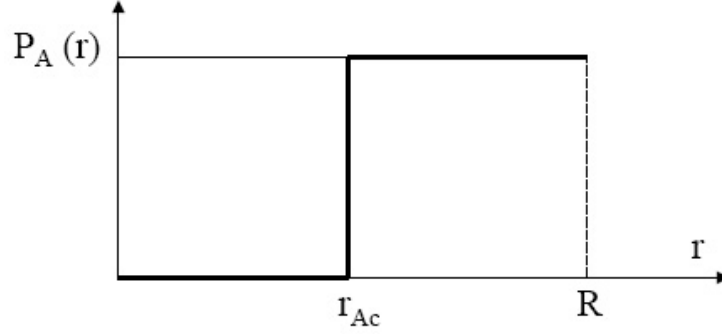


Figure 12. Probability to observe spots that appeared on a fluctuation of single amplitude  $A$ . The totality of these identical spots disappears at the same location  $r_{Ac}$ .

the propagation of the spots with the evolution of their amplitude probability  $Prob(A)$ . Assuming that torsional Couette flow has a critical amplitude curve as given in figure 2, one can calculate the probability  $P(r)$  for a spot to go through the circle of radius  $r$  by integrating  $P_A(r)$  over all the possible amplitude  $A$ :

$$\begin{aligned} P(r) &= \int_0^\infty P_A(r) Prob(A) dA \\ &= \int_{A_c(r)}^\infty Prob(A) dA \end{aligned} \quad (2)$$

To go further in the mathematical analysis, i.e. to compute the integral (2), it is necessary to assume that  $Prob(A)$  has a known mathematical expression. Unfortunately, our experiment does not permit to evaluate  $Prob(A)$ . However, as a first guess, and in order to illustrate furthermore our statistical theory for spots generation and disappearance, let us suppose that  $A$  has a Gaussian distribution as the generating fluctuations at the disc rim are due to external noise:

$$Prob(A) = \frac{1}{\sqrt{2\pi}\sigma_A} \exp\left[-\frac{(A - A_m)^2}{2\sigma_A^2}\right], \quad (3)$$

where  $A_m$  and  $\sigma_A$  are respectively the mean value and the standard deviation of the probability of perturbation amplitudes  $A$ . As already indicated, both can be functions of  $r$ . We then calculate explicitly  $P(r)$

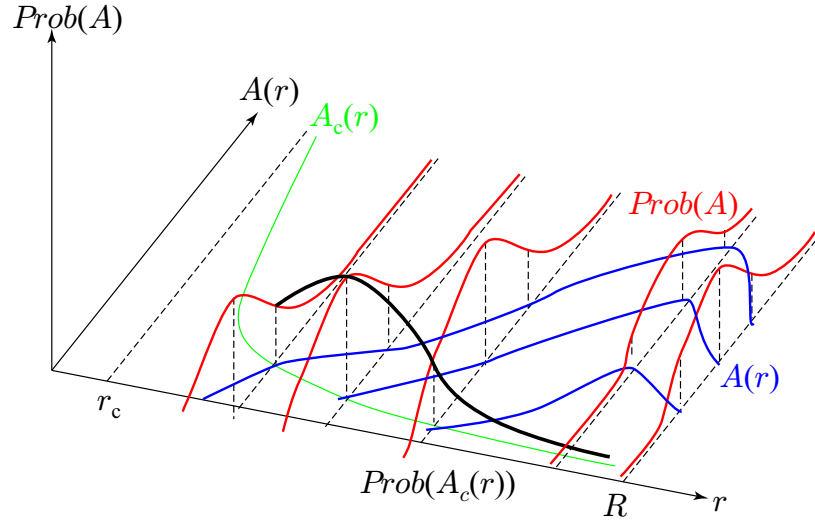


Figure 13. Schematic diagram of variation of  $Prob(A)$ , where intersection with  $A_c(r)$  represents  $Prob(A_c(r))$ .  $P(r)$  is the integration of  $Prob(A)$  from this limit  $A_c(r)$  to infinity.

as an error function:

$$\begin{aligned}
 P(r) &= \frac{1}{\sqrt{2\pi}\sigma_A} \int_{A_c(r)}^{\infty} \exp\left[-\frac{(A - A_m)^2}{2\sigma_A^2}\right] dA \\
 &= 1 - \frac{1}{\sqrt{2\pi}\sigma_A} \int_{A_c(r)}^{A_m(r)} \exp\left[-\frac{(A - A_m)^2}{2\sigma_A^2}\right] dA \\
 &= 1 - \text{erf}(X),
 \end{aligned} \tag{4}$$

with

$$X = \frac{(A_c(r) - A_m(r))}{\sqrt{2} \sigma_{A_c}(r)} \tag{5}$$

Figure 14 shows two examples where it can be verified that the functions  $P(r)$  are very close to error functions as predicted by the previous Gaussian model. The functions  $X(r)$  can be estimated by a direct inversion of the experimental curves  $P(r)$  of figure 14-a). They are represented in figure 14-b). Note that  $X(r)$  would be a strictly linear function of  $r$  if  $P(r)$  was exactly an error function of  $r$ , i.e. if  $Prob(A)$  was an exact Gaussian distribution. From the definition of  $X(r)$ , we can determine directly the mathematical expression of the stability curve  $A_c(r)$ . This function is in fact the only quantity that

characterizes the torsional Couette flow:

$$A_c(r) = A_m(r) + \sqrt{2} \sigma_{A_c}(r) X(r) \quad (6)$$

As one can see from equation 6, the behavior of the stability curve  $A_c(r)$  is a balance between functions  $X(r)$  and  $Prob(A)$ . But equation 6 is only valid if  $Prob(A)$  is a Gaussian function. And we just saw that this is not exactly the case. Thus, as a second guess, let us now suppose that  $Prob(A)$  is similar to the Poisson distribution that was measured for the temporal fluctuations of the total number of spots (see figure 7). This is very plausible as intense fluctuations are supposed to generate groups of many spots. Therefore, let us take the number of generated spots as the amplitude unit of perturbations. Let us now remark that  $P(r)$ , being by definition the probability of observing a spot at a position  $r$ , can also be seen as the integrated probability of spot disappearance at radius  $r$ .  $P(r)$  is indeed the sum of the total number of spots crossing the circle of radius  $r$  and disappearing at a smaller radius. Figure 15 shows the examples of the probability for spot disappearance  $\frac{dP(r)}{dr}$ , calculated from the experimental measurements of figure 14. As expected, the characteristic hump of a probability curve is found with a well defined maximum that corresponds in fact to the zero crossing of the  $X(r)$  function. Equation 5 shows that this location  $r_o$  corresponds to a radial position where  $A_c(r_o) = A_m(r_o)$ .  $r_o$  corresponds to a Reynolds number of about 3600. As explained before, if we take as an amplitude unit the number of spots, this Reynolds

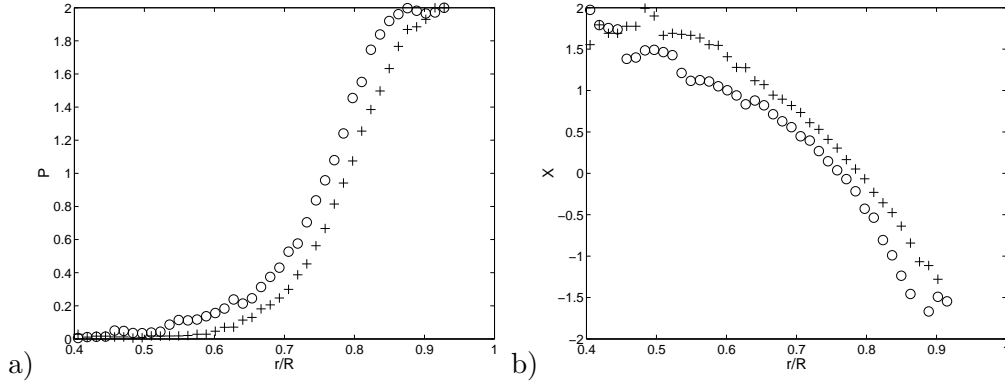


Figure 14. Two examples from the experiments for  $h = 2.0 \text{ mm}$  and  $\Omega = 150 \text{ rpm}$  (+) and for  $h = 2.6 \text{ mm}$  and  $\Omega = 110 \text{ rpm}$  (o) for the probability  $P(r)$  (normalized to 2)(a) and its associated function  $X(r)$  (b). We recognize the error function shape for  $P(r)$  although an exact fit would imply  $X(r)$  to be strictly linear which is obviously not the case.

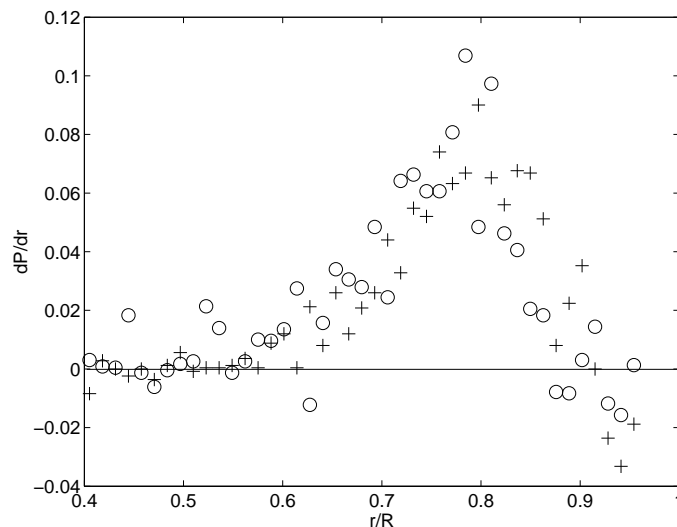


Figure 15. Experimental determination of the Probability for a spot to disappear as a function of the local position  $r/R$ , for  $h = 2.0 \text{ mm}$  and  $\Omega = 150 \text{ rpm}$  (+) and for  $h = 2.6 \text{ mm}$  and  $\Omega = 110 \text{ rpm}$  (o).

number corresponds to an amplitude able to generate 3 spots as given by the location of the maximum of the probability distribution in figure 7. The limit of the tails of the probability distributions are also other remarkable points that can be easily extracted from the experimental data. They correspond respectively to Reynolds numbers where the left tail of  $Prob(A)$  touches the stability curve around 4100 on its right side and around 2500 on its left side (see the diagram of figure 13). It appears that these limits are found to be reached for 1 spot and 18 spots on figure 7 where they represent the minimum and the maximum of the distribution. Therefore three points of the stability curve are exactly determined under the assumption that  $Prob(A)$  is the Poisson distribution as measured for the temporal fluctuation of the total number of spots. In order to get a sufficient number of points of the stability curve, this procedure can be continued for other probability values. One half and one quarter of the maximum of the probability distributions are thus chosen to complete the stability curve of torsional flow which is presented on figure 16-a). A best fit by a power law leads to a critical Reynolds number  $Re_c = 2140$  and a power  $\alpha = -3/2$ . As explained in the introduction, this power law exponent is in agreement with the values already observed or predicted in different shear flows.

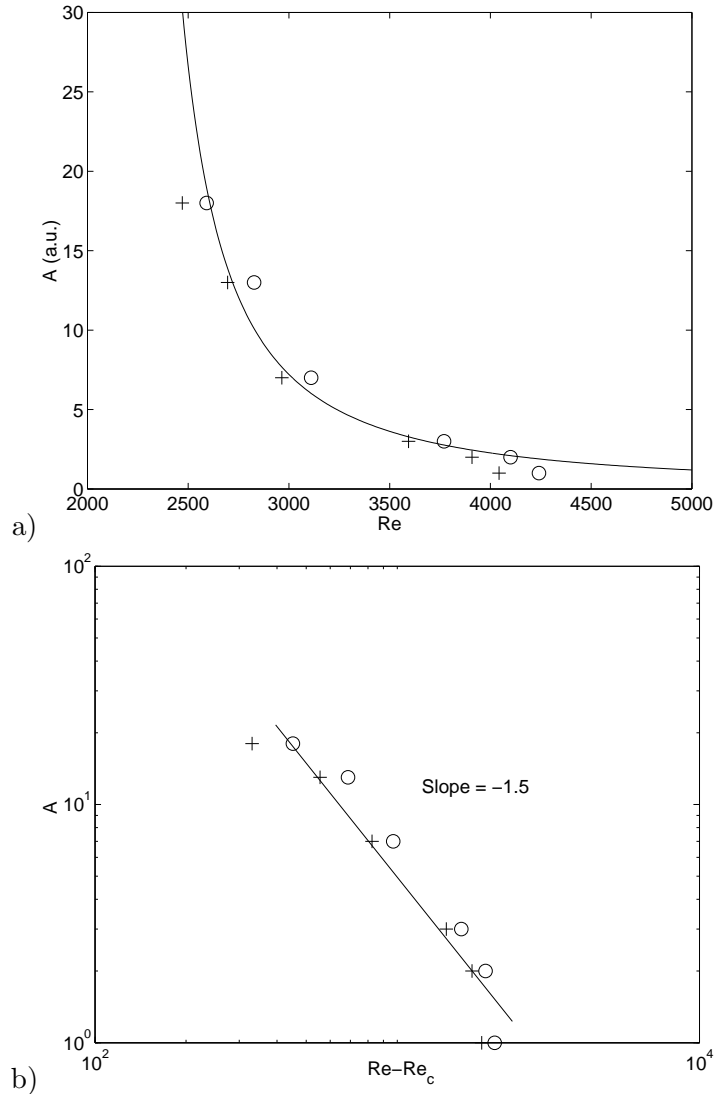


Figure 16. a) Stability curve  $f(Re)$  where the amplitude is considered to be proportional to the number of spots, b) the same in log-log scale where the best fit gives  $Re_c = 2140$  and  $\alpha = -1.5$ .  $f(Re)$  is determined for  $h = 2.0$  mm and  $\Omega = 150$  rpm (+) and for  $h = 2.6$  mm and  $\Omega = 110$  rpm (o).

## 5. Conclusion

We have performed a statistical analysis of the appearance of localized structures called "spots" in torsional Couette flow transition to turbulence. Visualizations using kalliroscope particles show that these spots have a horse-shoe vortical structure and are generated in the area

close to the gap between the rotating disc and the cylindrical vertical wall of the container. The narrower this radial gap is, the higher is the Reynolds number for spot appearance. We have then shown that the fluctuations of the total number of spots obey a Poisson statistical distribution in accordance with the expected statistical independence of each spot. A statistical model for the generation of spots and their propagation predicts an error function shape for the probability distribution of the spots as a function of the radial position. This result is exact in the case where the statistics of the amplitude generating spots is Gaussian. This general sigmoid shape of spot distribution is then confirmed by an image analysis of the flow but some deviations from the predicted exact error function shape are observed. Then, with the help of some very plausible assumptions (the number of generated spots is directly proportional to the amplitude of the perturbations) and by using the Poisson distribution previously measured for the number of spots, we extract from the measurements, the stability curve of torsional Couette flow. A best fit of the experimental data leads to a power law behavior:  $A_c = (Re - Re_c)^{-3/2}$ , with a critical Reynolds number  $Re_c = 2140$ . These values are compatible with values generally observed in subcritical transition to turbulence of shear flows.

### Acknowledgements

The authors would like to thank an anonymous reviewer whose comments greatly improve the quality of the original manuscript.

### References

1. A. Prigent, G. Grégoire, H. Chaté, O. Dauchot and W. van Saarloos, Large-scale finite-wavelength modulation within turbulent shear flows. *Phys. Rev. Lett.* 89 (2002) 014501.
2. D. Barkley and L.S. Tuckerman, Computational study of turbulent laminar patterns in Couette flow. *Phys. Rev. Lett.* 94 (2005) 014502.
3. D. Coles, Transition in circular Couette flow. *J. Fluid Mech.* 21 (1965) 385–425.
4. C.W. van Atta, Exploratory measurements in spiral turbulence. *J. Fluid Mech.* 25 (1966) 495–512.
5. A. Cros and P. Le Gal, Spatiotemporal intermittency in the torsional Couette flow between a rotating and a stationary disk. *Phys. Fluids* 14 (2002) 3755–3765.
6. O. Dauchot and F. Daviaud, Finite-amplitude perturbation and spots growth mechanism in plane Couette flow, *Phys. Fluids* 7 (1995) 335–352.
7. B. Dubrulle and S. V. Nazarenko, On scaling laws for the transition to turbulence in uniform shear flows. *Europhys. Letter* 27 (1994) 129–134.
8. G. Kreiss, A. Lundbladh and D.S. Henningson, Bounds for threshold amplitudes in subcritical shearflows. *J. Fluid Mech.* 270 (1994) 175–198

9. P. Manneville and M. Lagha, On the stability and decay of turbulent Couette flow. *Proceedings of the Euromech Fluid Mechanics conference 6*. Stockholm, June 26-30 (2006), p. 207. The abstract mentions an exponent equal to  $-2$ , but it was corrected to  $-1$  during oral presentation.
10. F. Waleffe, Transition in shear flows. Nonlinear normality versus non-normal linearity. *Phys. Fluids* 7 (1995) 3060–3066
11. B. Hof, A. Juel and T. Mullin, Scaling of the turbulence transition threshold in a pipe. *Phys. Rev. Lett.* 91 (2003) 244502.
12. J. Peixinho and T. Mullin, Finite amplitude stability curves in the transition to turbulence in pipe flow. *Proceedings of the Euromech Fluid Mechanics conference 6*. Stockholm, June 26-30 (2006), p. 355.
13. L. Schouveiler, P. Le Gal and M.P. Chauve, Instabilities of the flow between a rotating and a stationary disk. *J. Fluid Mech.* 443 (2001) 329–350.
14. A. Cros, E. Floriani, P. Le Gal and R. Lima, Transition to turbulence of the Batchelor flow in a rotor/stator device. *Eur. J. Mech. /B Fluids* 24 (2005) 409–424.
15. G. Gauthier, P. Gondret and M. Rabaud, On flow visualisation using reflective flakes. *Phys. Fluids* 10 (1998) 2147–2154.
16. S. Savas, On flow visualisation using reflective flakes. *J. Fluid Mech.* 152 (1985) 235–248.
17. N. Otsu, A thresholding selection method from gray-level histogram. *IEEE Transactions on System, Man, and Cybernetics* 9 (1979) 62–66.